Dynamic Modal Analysis of Monolithic Mode-Locked Semiconductor Lasers

Eugene A. Avrutin, *Member, IEEE*, John M. Arnold, and John H. Marsh, *Fellow, IEEE*

***Abstract*—We analyze the advantages and applicability limits of the mode-coupling approach to active, passive, hybrid, and harmonic mode-locking in diode lasers. A simple, computationally efficient numerical model is proposed and applied to several traditional and advanced laser constructions and regimes, including high-frequency pulse emission by symmetric and asymmetric colliding pulse mode-locking, and locking properties of hybrid mode-locked Fabry–Perot and distributed Bragg reflector lasers.**

***Index Terms*—Modeling, mode-locking (ML), optical pulses, semiconductor lasers, ultrafast optics.**

I. Introduction

MODE-LOCKING (ML) of monolithic semiconductor laser diodes (LDs) attracts considerable interest, first, for an increasing number of practical applications in microwave optoelectronics, (e.g., microwave over fiber), high-speed OTDM, and WDM communications (see [1] for an overview) and, second, from a purely scientific point of view, as an important prototype system in nonlinear dynamics and synergetics and as a manifestation of high-speed nonlinearities in active semiconductor media. Computationally efficient physically instructive theoretical models with predictive capabilities are, therefore, useful for a detailed understanding of the physics of these devices, analysis of their behavior and, ultimately, optimization of construction and operation regimes. A number of theoretical approaches to ML in LDs have been attempted in the last decade (see [1] for an overview). Most of these operate in the time domain and have progressed from modifications [2]–[4] of the classical semianalytical self-consistent pulse profile (SCP) theory (originally developed by H. Haus in the 1970s for gas and solid-state ML lasers), through intermediate level models [5], [6], to powerful distributed time-domain modeling (DTDM) techniques widely used recently for modeling dynamics and spectra of various LDs, including mode-locked lasers [1], [7]–[13]. However, SCP-type theories are plagued by a number of inaccuracies for semiconductor lasers [1], whereas DTDM modeling, while very powerful, can be taxing on computer resources and, being a purely numerical method, does not always provide physically instructive insight into interrelations between parameters. To achieve a combination of accuracy, physical transparency, and instructiveness in treating complex laser dynamics, it is very useful to supplement time-domain modeling by a *modal analysis* that treats the laser dynamics at least partly in *frequency* domain by means of (longitudinal) mode decomposition. The foundations of this approach for a generic class B mode-locked laser were developed by H. Haus at the same time as the SCP theory, with an emphasis on *active* ML [14]. Lau and co-workers [15]–[20] extended the approach to semiconductor lasers and successfully explained a number of important trends in the behavior of mode-locked lasers using simplified models that involved only three modes [15], [16], [20], or, in the opposite extreme, a continuum of modes [17]–[20]. This approach was extended by our team [1], [13], [21] and other authors [22], [23] to take into account a finite number of modes and to incorporate some specialized laser structures [24], [25]. So far, however, the progress in the time-domain analysis of ML LDs has not been matched by the modal decomposition approach, with no journal publication on this technique approaching the generality of the DTDM model. Here, we present the full version of the modal decomposition approach which: 1) is rigorously derived with the underlying approximations and limitations assessed; 2) includes some important effects (e.g., fast nonlinearities and group-velocity dispersion) neglected by other authors; 3) is applicable to a broad range of laser constructions [including harmonically mode-locked structures and distributed Bragg reflector (DBR) lasers] and operation regimes (active, passive, hybrid, and synchronous ML); and 4) is capable of describing both steady-state behavior and dynamics of mode amplitudes and phases. The organization of the paper reflects these features. Section II presents the derivation of the model and discusses the assumptions involved in this derivation. Section III presents the application of the model to simulate static and dynamic behavior of some traditional and novel laser constructions. Section IV contains the summary and conclusion.

Manuscript received January 6, 2003; revised June 23, 2003. This work was supported in part by the U.K. Engineering and Physical Sciences Research Council.

E. A. Avrutin is with the Department of Electronics, University of York, York YO10 5DD, U.K. (e-mail: eaa@ohm.york.ac.uk).

J. M. Arnold is with the Department of Electronics and Electrical Engineering, University of Glasgow, Glasgow G12 8LT, U.K.

J. H. Marsh is with the Department of Electronics and Electrical Engineering, University of Glasgow, Glasgow G12 8LT, U.K., and also with the Intense Photonics Ltd., Glasgow G72 OUX, U.K.

Digital Object Identifier 10.1109/JSTQE.2003.818845

II. Model

A. Slow and Fast Variables in Mode Decomposition

The principle of longitudinal mode decomposition is well known; it means that the time and space dependence of the lasing light in the cavity is represented in the generic form of

$$E_{3D}(\mathrm{r},t)=\Phi(x,y)\sum_k E_k(t)U_k(z,t)\times\exp\Big(i\big(\omega_k t+\psi_k(t)\big)\Big)+\text{c.c.}\quad(1)$$

where Φ is the transverse-lateral mode profile, and $E_{\rm k}$, ω_k, ψ_k, and $U_{\rm k}$ are amplitudes, frequencies, phases, and spatial profiles of longitudinal modes, respectively (strictly speaking, Φ can be also a function of k, albeit weak, because of waveguide dispersion). However, a meaningful definition of longitudinal modes and, therefore, of the functions U_k, for a realistic semiconductor laser is not entirely straightforward. Indeed, the laser is an open, inhomogeneous optical cavity with gain and loss. Moreover, in a multimode laser, the dielectric permittivity is always time-dependent, even during nominally continuous-wave operation, due to mode beating. Most papers on modal analysis of mode-locked LDs [15]–[22] used simple standing waves ($U_{\rm k} \sim \cos(\pi k z/L)$, where L is the cavity length) as a basis of mode decomposition. However, these are not true eigenmodes for an open laser cavity and, so, their use is mathematically unjustified, particularly for describing cavities other than a simple Fabry–Perot resonator (such as a DBR resonator or a coupled-cavity construction). An opposite approach to modes in semiconductor lasers involves calculating true, instantaneous mode profiles of the realistic cavity at each moment in time, using instantaneous local values of the complex dielectric constant. This approach was most fully developed [26] for single- (or dual) mode DFB lasers. To the best of our knowledge, it has not been applied to ML, though, in a recent paper, Feiste [27] has used it to analyze applications involving resonant modulation of DBR lasers, which may be seen as a special degenerate case of active ML. A generalization to fully rendered ML should be, in principle, straightforward. However, this technique, being exactly mathematically equivalent to DTDM modeling [27], is as general as DTDM—but, by the same token, tends to be no more, and sometimes less, computationally efficient [28]. Here, we use an intermediate approximation, which is more realistic and general than the simple standing-wave expansion but less cumbersome, if somewhat less general, than the true instantaneous mode calculation. We make use of the fact that in most multimode lasers, frequency distances between all adjacent modes are close to a nominal round-trip frequency $\Delta\Omega_0 = v_g/2L_{\rm c}$, $L_{\rm c}$ being the characteristic size of the laser cavity (the physical cavity length for a Fabry–Perot resonator, or the effective length, defined in Section III, for a DBR cavity), and $v_g = c/\eta_g$, the group velocity of light ($\eta_g = \eta + \omega \cdot \partial\eta/\partial\omega$ being the group refractive index in the waveguide). Then, we define a parameter (say, A) as *slow* if its temporal evolution is much slower than the round-trip frequency

$$\left|\frac{\partial A}{\partial t}\right| \ll |\Delta\Omega_0 A| \tag{2}$$

and *fast* otherwise (i.e., when $|\partial A/\partial t| \sim |\Delta\Omega_0 A|$). It is then natural to describe all the fast laser dynamics in frequency-domain terms via the decomposition (1) and all the slow dynamics in time domain through the temporal dynamics of the parameters $E_{\rm k}$, $\psi_{\rm k}$, and $U_{\rm k}$. The mode profiles $U_{\rm k}$ then describe the open and inhomogeneous cavity and are instantaneous, as in [26], [27]—but only on the slow time scale, which makes for much more efficient calculations. The model is essentially the same as that used in our earlier work [13], [21], [24], but will be described here, first, because our previous papers presented the model without derivation and, second, because the present version is more general than those used before and applies to more laser constructions.

B. Field and Polarization in the Laser. Weak Modulation and Nonlinearity Approximation

Concentrating on longitudinal effects, we shall assume that strong built-in index guiding ensures a single transverse/lateral mode with a profile $\Phi(x, y)$ as in (1). Then, we may start with the one-dimensional wave equation in the general form

$$\frac{\partial^2}{\partial z^2}E - \frac{1}{c^2}\frac{\partial^2}{\partial t^2}[\hat{\eta}^2 E] = \frac{1}{c^2}\frac{\partial^2}{\partial t^2}\Gamma P \tag{3}$$

Here, $E(z,t)$ the longitudinally varying field ($E_{3D}(x,y,z,t) = \Phi(x,y)E(z,t)$), measured in units such that its square equals the photon density (averaged over an optical oscillation period); $\eta(z)$ the effective waveguide refractive index that describes the *nonresonant* (built-in) dielectric properties, including built-in Bragg grating(s), if any. Finally, P is the *resonant* component of the dielectric polarization which is associated with the lasing transition and restricted to the active layer, hence, the optical confinement factor Γ. The symbol $\hat{}$ over a parameter notation means that the corresponding parameter is, strictly speaking, dispersive (optical frequency dependent) and, in the time domain formalism of (3), should be understood as an operator, e.g., $\hat{\eta}E = \mathrm{FT}^{-1}[\eta(z,\omega)\cdot \mathrm{FT}(E)]$, where FT and FT^{-1} are the direct and inverse Fourier transforms between time (t) and optical frequency (ω) domains. In realistic lasers, the material dispersion tends to be comparatively weak (in the sense that the relative variation in the parameters over the lasing spectrum is small) but it is retained here, since group velocity dispersion has been shown to be of some importance in some mode-locked laser constructions [1], [12]. Next, we introduce the rotating wave notation

$$E(z,t) = e^{i\omega_{\rm ref}t} \times \left(E_r(z,t)e^{-i\int\beta_{\rm ref}dz} + E_l(z,t)e^{i\int\beta_{\rm ref}dz}\right) + \text{c.c.} \tag{4}$$

where $\omega_{\rm ref}$ and $\beta_{\rm ref} = \eta(z)\omega_{\rm ref}/c$ are the reference optical frequency and longitudinal wave vector, respectively [the latter, as in [27], is allowed a (weak) z-dependence for convenience, to allow slightly different β_{ref} values to be assigned to cavity sections of different physical nature, i.e., active sections, passive sections, grating sections, saturable absorbers etc.], and E_r and E_l are the "slow amplitudes" ["slow" in the sense of $|(\partial/\partial t)E_{r,l}| \ll |\omega E_{r,l}|$; $|(\partial/\partial z)E_{r,l}| \ll |\beta E_{r,l}|$ though not necessarily in the sense of (2)] of right- (forward-) and left- (reverse-) propagating fields, respectively. It is then convenient, following the notations of [26], [27], [29], to introduce a two-dimensional "vector" $\boldsymbol{E}$ defined as

$$\boldsymbol{E}(z,t) = \left\{\begin{array}{c} E_r(z,t) \\ E_l(z,t) \end{array}\right\}. \tag{5}$$

Similar "vector" notations may be introduced for the resonant polarization P. Let us now consider this latter parameter in more detail. It is well known that the main dynamic variable that describes the active layer medium and, thus, parameterizes

the polarization $\boldsymbol{P}$ is the free carrier density $N(z,t)$. For subsequent analysis, we shall separate components of this variable varying with time at different time scales

$$N(z,t) = N_0(z,t) + \sum_{m=1}^{\infty} N_m(z,t) e^{im\Delta\Omega_o t} + \text{c.c.} \qquad (6)$$

In (7), N_0 is the slow component of N and the rest of the terms in the series are fast, though all the amplitudes N_m, $m = 0, 1, 2\ldots$ are slow quantities. Physically, the fast terms represent the density response to longitudinal mode beating (important in passive ML) and/or to external resonant modulation (e.g., in active ML). In multigigahertz lasers, we may expect these quantities to be small

$$|N_m| \ll N_0, \quad m = 1, 2\ldots. \qquad (7)$$

since the characteristic time of the relaxation of N is much longer than $1/\Delta\Omega_0$. In the resonant polarization P, we can then separate several terms of different physical nature, namely

$$\boldsymbol{P} = \boldsymbol{P}_0 + \boldsymbol{P}_{\text{qe}} + \boldsymbol{P}_{\text{ne}} + \boldsymbol{P}_{\text{rm}} \qquad (8)$$

The first term P_0 is associated with the slow component N_0 of the carrier density and may be written as

$$\boldsymbol{P}_0 = \widehat{\Delta\varepsilon}(N_0)\boldsymbol{E} \approx \left(-\frac{i\eta c}{\omega_{\text{ref}}}\hat{g}(N_0) - \eta\widehat{\Delta\eta}(N_0)\right)\boldsymbol{E} \qquad (9)$$

where $\Delta\varepsilon(N,\omega)$ is the interband component of the dielectric constant, which includes the gain $g(N,\omega)$ and the density-dependent refractive index $\Delta\eta(\omega)$. The polarization P_0 does not depend on the light intensity directly, only parametrically through the dynamics of N_0. We shall, therefore, refer to it as the *quasi-linear* term. The next two terms in (8) then describe the *nonlinear* polarization, *explicitly* dependent on the light intensity. The former of the two, *quasi-equilibrium* term, P_{qe}, is associated with the fast oscillations $N_m(m = 1, 2\ldots)$ of total carrier density. The following, *nonequilibrium* term P_{ne}, is introduced to describe fast optical nonlinearities. These describe nonlinear optical response of the active medium due to effects related to the deviation of the energy distribution of carriers from equilibrium at constant total local density N. Such effects include spectral hole burning, dynamic carrier heating, well-barrier nonequilibrium, and, for the case of quantum well-saturable absorbers, kinetics of exciton ionization. The final term in (8) P_{rm} is due to external resonant modulation of the dielectric constant at or near the round-trip frequency and/or its harmonics and is only present in active, hybrid, or synchronous ML. To achieve sufficient analytical progress in the model, we need to treat all three nonlinear and modulation-induced polarization terms as small corrections to the quasi-linear term. This *weak nonlinearity and modulation* approximation, although not universal, is sufficient for treating many laser constructions and regimes of practical interest. Indeed, the small correction nature of the *quasi-liequilibrium* term P_{qe}, follows from (7); the fast nonlinearities that lead to the *nonequilibrium* term P_{ne} are well known to be relatively weak in most practical cases; and, finally, strong-signal *modulation* is hardly practical at the multigigahertz frequencies of interest here (nor is it necessary to achieve ML). In the derivation below, we assume, therefore

$$|\Delta P| \ll \left|P_{(0)}\right| \qquad \Delta P = P_{\text{qe}} + P_{\text{ne}} + P_{\text{rm}}. \qquad (10)$$

C. Modes of the Laser Cavity

Now, we substitute (8) and (9) into (3) and rewrite (3) with the aid of (4) in terms of amplitude vectors (5). The result is conveniently expressed in a matrix operator notation as in [26] and [27]

$$-i\frac{\partial \boldsymbol{E}}{\partial t} = \widehat{\mathbf{H}}\boldsymbol{E} + \frac{\omega_{\text{ref}}}{2\eta\eta_g}\boldsymbol{P}. \qquad (11)$$

with the matrix operator $\widehat{\mathbf{H}}$ defined as

$$\widehat{\mathbf{H}}\boldsymbol{E} = v_g\left[i\begin{pmatrix}1 & 0\\ 0 & -1\end{pmatrix}\frac{\partial}{\partial z} - \begin{pmatrix}\widehat{\Delta\beta}(z,t) & K_{rl}(z)\\ K_{lr}(z) & \widehat{\Delta\beta}(z,t)\end{pmatrix}\right]\cdot\boldsymbol{E} \qquad (12)$$

Here,

$$\widehat{\Delta\beta}(z,t)(z,t) = \widehat{\beta}(z,t) - \beta_{\text{ref}} \approx \frac{\omega_{\text{ref}}}{c}\widehat{\Delta\beta}(z,t) + \frac{i}{2}\hat{g}(z,t)$$

defines the local complex wavevector. The relation between its real and imaginary parts may, to a first order, be approximated using the Henry linewidth enhancement factor α: $\Delta\eta = -\alpha gc/\omega_{\text{ref}}$. K_{rl} and K_{lr} stand for distributed coupling between right- and left-propagating waves ($K_{\text{rl}} = K_{\text{lr}} = 0$ everywhere except DFB or DBR sections, if any). To define the operator $\widehat{\mathbf{H}}$ fully, (12) is completed with boundary conditions at the facets

$$E_r\left(-\frac{L}{2}\right) = \rho_l E_l\left(-\frac{L}{2}\right) \qquad E_l\left(\frac{L}{2}\right) = \rho_r E_r\left(\frac{L}{2}\right) \qquad (13)$$

where $\rho_{r,l} = r_{r,l}\exp(-i2\int_0^{\pm L/2}\beta_{\text{ref}}dz)$ are effective right and left reflectances for slow amplitudes (generally speaking, they differ from physical reflectances $r_{l,r}$ by random phase factors, though this is only important in complex laser constructions such as grating lasers, or compound-cavity structures which also need an additional boundary condition [24]).

We then choose the eigenfunctions $U_k(z,t)$ of the operator $\widehat{\mathbf{H}}$, defined by the expression

$$\widehat{\mathbf{H}}\boldsymbol{U}_{\mathbf{k}} = \widetilde{\Omega}_k\boldsymbol{U}_k \qquad (14)$$

as the basis functions of the expansion. The complex eigenvalues $\widetilde{\Omega}_k = \Omega_k - i\gamma_k$ describe the (relative) mode frequency Ω_k and the net modal amplitude gain γ_k. To project the wave equation on the basis of the functions $\boldsymbol{U}_k(z,t)$, we introduce the inner product of two functions defined as [26], [27], [29]

$$\boldsymbol{U}^*\boldsymbol{V} = \int_{-\frac{L}{2}}^{\frac{L}{2}} \text{dz}(U_r V_l + U_l V_r) \qquad (15)$$

and use the properties of the operator $\widehat{\mathbf{H}}$ and its eigenfunctions and eigenvectors established in the literature [26], [27], [29]. The most important of these properties are the orthonormality

$$\boldsymbol{U}_k{}^*\boldsymbol{U}_m = \delta_{\text{km}} \qquad (16)$$

(the unity factor at the Kronecker symbol being ensured by appropriate normalization of U_k) and the completeness of the set

$$\boldsymbol{W}(z,t) = \sum_{k=-\infty}^{\infty} f_k(t)\boldsymbol{U}_k(z,t) \tag{17}$$

[for any field profile $\boldsymbol{W}$ satisfying the boundary conditions as in (13)]. In laser constructions used for ML, we may expect that the frequency difference between the two adjacent modes is never far detuned from the "nominal" intermodal interval $\Delta\Omega_0$

$$|\Omega_k - \Omega_{k-1} - \Delta\Omega_0| \ll \Delta\Omega_0$$

and, moreover, that $|\gamma_k| \ll \Delta\Omega_0$ for all modes. By numbering the eigenfunctions so that the mode number zero is the one nearest to the reference frequency $\omega_{\rm ref}$ and choosing $\omega_{\rm ref}$ appropriately, we may also ensure that $|\Omega_0| \ll \Delta\Omega_0$. Then, we may rewrite the solution (1) of (11) in "vector" notations and with $\omega_k = k\Delta\Omega_0 + \omega_{\rm ref}$

$$\boldsymbol{E}(z,t) = \sum_k E_k(t)\boldsymbol{U}_k(z,t)\exp\Big(i\big(k\Delta\Omega_0 t + \psi_k(t)\big)\Big) + \text{c.c.} \tag{18}$$

Furthermore, we note that in a mode-locked laser, the modes are shifted from their "cold-cavity" positions and the intermodal interval is only approximately equal to the nominal value $\Delta\Omega_0$. This means that even in the steady-state ML regime, the phases $\psi_k(t)$ vary (linearly) with time. To get a more instructive model, it is convenient to recalibrate the phases

$$\psi_k(t) = \varphi_k(t) + \int \Big(k\big(\Delta\Omega(t) - \Delta\Omega_0\big) + \Omega_c(t)\Big)dt \tag{19}$$

Here, $\Delta\Omega(t) - \Delta\Omega_0$ and $\Omega_c(t)$ are dynamic corrections to the intermodal interval and the position of the reference (zero) mode, respectively, defined in such a way that in a steady-state multimode regime such as ML, the recalibrated phases φ_k are constant. Apart from this requirement and the provision that $|\Omega_c| \ll \Delta\Omega_0$, $|\Delta\Omega - \Delta\Omega_0| \ll \Delta\Omega_0$, the definitions of the calibration functions $\Delta\Omega(t)$ and $\Omega_c(t)$ are largely arbitrary and, within the numerical accuracy limits, should not affect the "measurable" parameters given by the model (such as mode intensities). Our method of estimating these functions will be discussed below.

D. Rate Equations for Complex Mode Amplitudes. Moderate-Dispersion Approximation

Substituting the mode decomposition in the form of (18) into (11) for the light field results in a system of rate equations which are most compactly expressed in terms of complex mode amplitudes

$$\begin{aligned}\widetilde{\mathrm{E}}_k(t) &= E_k(t)e^{\mathrm{i}\varphi}k^{(t)}\\ \frac{d}{dt}\widetilde{\mathrm{E}}_k &\approx i(\widetilde{\Omega}_k - k\Delta\Omega - \Omega_c)\widetilde{\mathrm{E}}_k\\ &\quad + \frac{i\omega_{\rm ref}}{2\eta\eta_g}\left\{(\boldsymbol{U}_k{}^*\Delta\boldsymbol{P})\,e^{-i\int(k\Delta\Omega+\Omega_c)\mathrm{dt}}\right\}_{\rm slow}.\end{aligned} \tag{20}$$

Here, the first term describes the starting approximation, neglecting the modulation and nonlinear polarization terms $\Delta\boldsymbol{P}$. As can be expected from the definition of the eigenmodes $\boldsymbol{U}_k$, this approximation corresponds to the case of *uncoupled* modes as the first term includes only parameters of the same kth mode. The modes are only coupled by the second term that includes ΔP. Using the weak nonlinearity condition (10), we treat these terms in the first order of the perturbation theory, using $\boldsymbol{U}_k$ as the starting approximation eigenfunctions. The subscript slow means the slow, resonant component (the fast, nonresonant, components are corrections of a higher order due to their oscillating nature). The same weak nonlinearity condition (10) means that the nonlinear terms $P_{\rm qe}$ and $P_{\rm ne}$ in (10) and (20) need include only the lowest, third, order nonlinearities. In the present version of the model, we shall neglect wavelength-scale nonlinear effects such as self-induced gratings. Then, the general form for the nonlinear terms is

$$\begin{aligned}P_{\rm qe(ne)} = 4\pi \sum_{k_1,k_2,k_3} &\chi^{(3,\rm qe(ne))}_{k_1,k_2,k_3}\widetilde{\mathrm{E}}_{k_1}\widetilde{\mathrm{E}}_{k_2}\widetilde{\mathrm{E}}^*_{k_3}\left\{U_{k_1}U^*_{k_3}\right\}_{\rm env}\\ &\times U_{k_2}e^{i\int((k_1+k_2-k_3)\Delta\Omega+\Omega_c)\mathrm{dt}}\end{aligned} \tag{21}$$

In (21), $\chi^{(3,\rm qe(ne))}_{k_1k_2k_3}$ are the quasi-equilibrium and nonequilibrium contributions to effective third-order nonlinear susceptibilities $\chi^{(3,)}_{k_1k_2k_3} = \chi^{(3,\rm qe)}_{k_1k_2k_3} + \chi^{(3,\rm ne)}_{k_1k_2k_3}$ and the subscript env means the spatially slow envelope, with wavelength-scale nonuniformities averaged out. Then, the corresponding terms in (20) may be rewritten as

$$\begin{aligned}&\left\{\boldsymbol{U}_k{}^*(\boldsymbol{P}_{\rm qe} + \boldsymbol{P}_{\rm ne})e^{-ik\int\Delta\Omega dt}\right\}_{\rm slow}\\ &\quad = 4\pi\sum_{k_1,k_2,k_3} X^{(3)}_{k_1k_2k_3}\widetilde{\mathrm{E}}_{k_1}\widetilde{\mathrm{E}}_{k_2}\widetilde{\mathrm{E}}^*_{k_3}\delta_{k_1+k_2-k_3,k}\end{aligned} \tag{22}$$

Here,

$$\mathrm{X}^{(3)}_{k_1k_2k_3} = \mathbf{U}_{k_1+k_2-k_3}{}^*\left(\chi^{(3)}_{k_1k_2k_3}\left\{U_{k_1}U^*_{k_3}\right\}_{\rm env}\mathbf{U}_{k_2}\right) \tag{23}$$

The rate equations (20) with the nonlinear terms in the form of (22) are formally similar to the classical equations derived by Lamb [30] for gas and solid-state lasers and, later, empirically introduced for simplified modeling of the regime known as frequency-modulation locking in homogeneously pumped semiconductor lasers [31], [32]. In a detailed self-consistent model of a multimode or mode-locked laser, however, equations in such a form would present some difficulties. This is because of the task of parameterizing the third-order permittivities $\chi^{(3)}_{k_1k_2k_3}$ (23) for all the values of the three indexes (in [31], [32], empirical constants were used for these values). Even if the nonlinearity coefficients are calculated microscopically, the right-hand side of (23) contains cumbersome double summation. The problem is, however, greatly simplified if we use the *moderate dispersion* condition which involves retaining the dispersion (mode number dependence) only of the quasi-linear properties (such as the mode eigenvalues $\widetilde{\Omega}_k = \Omega_k - i\gamma_k$) and neglecting dispersion of nonlinearities. This is a reasonable assumption since both the nonlinearity and the dispersion are treated as small corrections and their *joint* effect is, therefore, a correction of the next order. To make full use of the moderate dispersion approximation, we need to validate it, not only for

the active medium properties, but also for those of the laser cavity. Namely, we need to ensure that the spatially averaged product of two modes depends only on the frequency interval between the modes but not on their absolute spectral positions

$$\left\{U_k U_{k+m}^*\right\}_{\rm env} = \Xi_m = \Xi_{-m} \neq f(k) \tag{24}$$

This is equivalent to neglecting the spectral (or mode number) dependence of the spatially slow envelope of a mode profile $\{U_k\}_{\rm env}$. For an idealized closed cavity, with U_k defined as standing waves, the relation (24) holds universally and exactly. In a realistic cavity, with mode eigenfunctions defined by (14), this relation is only approximate. Still, for simple Fabry–Perot cavities, (24) follows directly from the condition of moderate material dispersion. With more complex, frequency-selective, resonators, such as DBR or compound cavities, (24) is less obvious and may, in general, be inaccurate. However, in such frequency-selective cavities, the modes that are selected for laser operation (for example, modes within the Bragg stopband in a DBR laser) by definition have close net gains γ_k, which also implies a similar spatial structure (see Appendix). Modes that have considerably different spatial profiles (such as the modes outside the Bragg stopband in a DBR laser) experience a lower net gain and are, therefore, not important in the lasing spectrum. Therefore, with some caution, we may extend the use of (24) to coupled-cavity and DBR lasers.

With these reservations, the quasi-equilibrium polarization $P_{\rm qe}$ may be derived from the rate equation for the carrier density N. With E in the "square root of photon density" units

$$\frac{\partial N(z,t)}{\partial t} = \frac{J}{\rm ed} - \frac{N}{\tau_N(N)} - v_g {\rm Re}(E^* \hat{g} E) + D\frac{\partial^2 N}{\partial z^2} \tag{25}$$

Assuming that the only role of carrier diffusion [the last term in (25)] is to smooth out wavelength-scale variations of N, and using the moderate-dispersion and weak-nonlinearity approximations, we may split this equation into separate relations for slow and fast components of $N(z,t)$. For the slow component $N_0(z,t)$, the result is a distributed rate equation

$$\frac{dN_0(z,t)}{\rm dt} \approx \frac{J}{\rm ed} - \frac{N_0}{\tau_N(N_0)} - v_g \Xi_0(z) \sum_{k=-\infty}^{\infty} g_k E_k^2. \tag{26}$$

For the (small) fast components, collecting the resonant terms gives

$$\frac{dN_m(z,t)}{\rm dt} + im\Delta\Omega N_m \approx -\frac{N_m}{\tau_\Sigma} - v_g g \cdot \Xi_m \sum_k \widetilde{\rm E}_k^* \widetilde{\rm E}_{k+m} e^{-im\int(\Delta\Omega - \Delta\Omega_0)dt}. \tag{27}$$

Here, J is the pumping current density, $\tau_N(N)$ is the carrier lifetime, and the effective recombination time $\tau_\Sigma(z,t)$ is the inverse total recombination rate, including both the nonstimulated recombination described by $\tau_N(N)$ and the stimulated recombination due to lasing

$$\frac{1}{\tau_\Sigma(z,t)} = \frac{d}{dN_0}\left(\frac{N_0}{\tau_N(N_0)} + v_g \Xi_0(z) \sum_{k=-\infty}^{\infty} g_k E_k^2\right). \tag{28}$$

Noting that the amplitudes $N_m(z,t)$ are slow variables, and making use of (2), we can neglect time derivatives in (27), yielding

$$N_m(z,t) e^{im\int(\Delta\Omega - \Delta\Omega_0){\rm dt}} \approx -v_g g \cdot \Xi_m \frac{\tau_\Sigma}{1 + im\tau_\Sigma \Delta\Omega} \sum_k \widetilde{\rm E}_k \widetilde{\rm E}_{k+m} \tag{29}$$

The effective permutation in the dielectric permittivity caused by this small [due to (7)] variation of carrier density has a complex amplitude of $\Delta_\chi = (c\eta/4\pi\omega)\cdot(\partial g/\partial N)(i-\alpha)N_m$. Substituting this into (21)–(23), we can obtain an expression for the quasi-equilibrium part of the small-signal third-order dielectric permittivity

$$\chi^{(3,q)}_{k_1 k_2 k_3} = -v_g g \frac{c\eta}{4\pi\omega} \cdot \frac{\partial g}{\partial N}(i-\alpha)\frac{\tau_\Sigma}{1 - i(k_1 - k_3)\tau_\Sigma \Delta\Omega} \tag{30}$$

where c and n are the velocity of light and the effective refractive index, respectively, and $k_3 \neq k_1$. In the moderate dispersion approximation, $\chi^{(3,q)}_{k_1 k_2 k_3}$ does not depend on the middle index k_2. Since the nonequilibrium components of the fast polarization, like the quasi-equilibrium terms, have origin in pulsations of population inversion, their contribution to $\chi^{(3)}$ may be written in the same functional form

$$\chi^{(3,ne)}_{k_1 k_2 k_3} = -\frac{c^2\eta}{4\pi\omega} \cdot \frac{i\varepsilon}{1 - i(k_1 - k_3)\tau_{nl}\Delta\Omega}. \tag{31}$$

Here, the complex value ε has the dimension of $1/E^2 =$ cm^3, and the physical meaning of a characteristic coefficient of mode interaction due to mode beating (four-wave mixing nonlinearity coefficient). $\tau_{\rm nl}$ is the characteristic type of relaxation for the dominant type of nonlinearity (e.g., carrier thermalization time for spectral hole burning or cooling time for dynamic carrier heating; both typically have subpicosecond values). If more than one type of nonlinearities is significant for the laser material studied, the nonequilibrium term can be generalized in the form of a sum of corresponding terms. We note that the functional form (31) for the fast optical nonlinearities implies, apart from the moderate dispersion, also adiabatic exclusion of polarization, or neglect of any electron-hole coherence. This is valid when $\tau_{\rm nl} \gg T_2$, where T_2 is the characteristic dephasing time for the electron-hole transitions (typically in semiconductors under lasing conditions, $T_2 \sim$ 50–100 fs). For the case of carrier heating nonlinearities, this is a good approximation as in this case $\tau_{\rm nl} \sim$ 300–700 fs. For spectral hole burning and related nonlinearities ($\tau_{\rm nl} \sim$ 100 fs), the adiabatic exclusion of polarization is more tenuous but is still known to be a reasonable approximation [33]. The nonlinearity coefficient ε and the response time $\tau_{\rm nl}$ may be calculated microscopically, as can gain/absorption coefficients and refractive index variation, but this is beyond the scope of this paper. Note that (31),

unlike (30), holds also for $k_1 = k_3$, when it describes gain/absorption cross-saturation if $k_1 = k_3 \neq k_2$ or self-saturation if $k_1 = k_3 = k_2$.

Substituting (30) and (31) into (20), we obtain the mode coupling equations in the form [13], [21]

$$\frac{d}{\mathrm{dt}}\widetilde{\mathrm{E}}_k(t) \approx i\left(\widetilde{\Omega}_k - \omega_k^n\right)\widetilde{\mathrm{E}}_k(t) + \sum_m G_m(t)\widetilde{\mathrm{E}}_{k+m}(t) \quad (32)$$

Here, the real parameter

$$\omega_k^n = k\Delta\Omega + \Omega_c \quad (33)$$

is the recalibrated "nominal" frequency assigned to the mode, and the complex values

$$\begin{aligned} G_m = \frac{v_g}{2L}\int_{-\frac{L}{2}}^{\frac{L}{2}} \mathrm{dz}\cos\left(\frac{m\pi}{L}\left(z+\frac{L}{2}\right)\right) \\ \times\left\{\Xi_m(z)\left(-g(z)\sum_k \widetilde{\mathrm{E}}_k\widetilde{\mathrm{E}}^*_{k+m}\right)\right. \\ \cdot\left[\frac{v_g(1+i\alpha)\left(\frac{\partial g}{\partial N}\right)\tau_\Sigma}{1-im\Delta\Omega\tau_\Sigma} + \frac{\varepsilon}{1-im\Delta\Omega\tau_{nl}}\right] \\ \left. + a_{\mathrm{mod}}(z)(1+i\alpha_{\mathrm{mod}})\right\} \end{aligned} \quad (34)$$

are the mode coupling coefficients ($m \neq 0$, note that in the notations used, each G_m is associated with N_{-m} rather than N_m). The first term in the figure braces describes the coupling via nonlinearity, and the second term, via external modulation. In this term, $a_{\mathrm{mod}}(z,t)$ is the amplitude of the external modulation of optical absorption (we assume that electrooptical modulation is used as this is much more efficient than current modulation [1]), and the linewidth enhancement factor α_{mod} defines the chirp of the modulator. In deriving (34), we have used the moderate dispersion condition to approximate

$$\begin{aligned} U_{kl}U_{k+m,r} + U_{kr}U_{k+m,l} \approx& \frac{1}{L}\cos\left(v_g(\Omega_{k+m} - \Omega_k)\left(z+\frac{L}{2}\right)\right) \\ \approx& \frac{1}{L}\cos\left(\frac{m\pi}{L}\left(z+\frac{L}{2}\right)\right). \end{aligned} \quad (35)$$

The mode coupling equation in the form of (32) contains only single summation in the right-hand side, as opposed to the double summation in (20) and (22). In a practical calculation, the integration over z in (34) has to be performed by subdividing the length of the laser cavity into sections in which the parameters such as the carrier density N_0 (and, by implication, the light intensity profile Ξ_0) can be treated as constant values, averaged over the length of the section. Here, we shall use the simplest approximation of only two sections coinciding (or nearly coinciding, to allow for the imperfect electrical isolation) with the two physically distinct regions in the cavity—the amplifier and the saturable absorber—though the model can be readily generalized with sections further subdivided to improve the accuracy. Space averaging gives for the coupling coefficients

$$\begin{aligned} \frac{2G_m}{v_g} =& \left(\sum_k \widetilde{\mathrm{E}}_k\widetilde{\mathrm{E}}^*_{k+m}\right) \\ &\cdot\left\{\xi_m^{(a)}a\left[\frac{v_g(1+i\alpha_A)\cdot A_A\cdot\tau_{\Sigma a}}{1-im\Delta\Omega\tau_{\Sigma a}} + \frac{\varepsilon_A}{1-im\Delta\Omega\tau_{nl}^{(a)}}\right]\right. \\ &\left. -\xi_m^{(g)}g\left[\frac{v_g(1+i\alpha_G)\cdot A_G\tau_{\Sigma g}}{1-im\Delta\Omega\tau_{\Sigma g}} + \frac{\varepsilon_G}{1-im\Delta\Omega\tau_{nl}^{(g)}}\right]\right\} \\ &+\Delta a_m(1+i\alpha_{\mathrm{mod}})\xi_m^{(\mathrm{mod})}. \end{aligned} \quad (36)$$

Here, we have introduced the overlap factors

$$\xi_m^{(g)} = \int_{(g)} \mathrm{dz}\Xi_m(z)\cos\left(\frac{m\pi}{L}\left(z+\frac{L}{2}\right)\right) \quad (37a)$$

$$\xi_m^{(a)} = \int_{(a)} \mathrm{dz}\Xi_m(z)\cos\left(\frac{m\pi}{L}\left(z+\frac{L}{2}\right)\right) \quad (37b)$$

$$\xi_m^{(\mathrm{mod})} = \int_{(\mathrm{mod})} \mathrm{dz}D_m(z)\cos\left(\frac{m\pi}{L}\left(z+\frac{L}{2}\right)\right) \quad (38)$$

with the integration in (37) being over the length of the gain or saturable absorber section and in (38) over the length of the modulator section [for some hybridly mode-locked lasers, the absorber doubles as the modulator, in which case, the limits of integration in (38) are the same as in (37b)]. The function $D_m(z)$ is the dimensionless spatial profile of the external modulation at or around the frequency of $m\Delta\Omega$ and, finally, Δa_{m} stands for the absorption modulation amplitude $a_{\mathrm{mod(m)}}(z) = \Delta a_{\mathrm{m}} D(z)$. In the special case of $m = 0$, the parameter G describes, not mode coupling, but self- and cross-saturation of gain and saturable absorption

$$G_0 = v_g S\cdot\left\{\xi_0^{(a)}a\varepsilon_A - \xi_0^{(g)}g\varepsilon_G\right\} \quad (39)$$

where $S = \sum_{k=-M/2}^{M/2} E_k^2$ is the total light intensity and the moderate dispersion approximation has been used to apply the same nonlinearity parameters for self- and cross-saturation. For the average (slow) carrier densities in the gain (N_g) and saturable absorber (N_a) sections, space averaging of (26) yields rate equations in the form

$$\frac{dN_g(t)}{\mathrm{dt}} \approx \frac{J}{ed} - \frac{N_g}{\tau_g(N_g)} - v_g\frac{\xi_0^{(g)}L}{L_g}\sum_{k=-\frac{M}{2}}^{\frac{M}{2}} g_k E_k^2 \quad (40)$$

$$\frac{dN_a(t)}{\mathrm{dt}} \approx -\frac{N_a}{\tau_a} + v_g\frac{\xi_0^{(a)}L}{L_a}\sum_{k=-\frac{M}{2}}^{\frac{M}{2}} a_k E_k^2. \quad (41)$$

These are the multimode equivalent of modified rate equations used by one of the authors [34] for modeling self-pulsating tandem lasers. The values of the carrier densities N_g and N_a are used to calculate space-averaged total recombination rates $1/\tau_{\Sigma_g}$ and $1/\tau_{\Sigma_a}$ in (34).

E. Equations for Numerical Modeling

The equations (32), (40), and (41) form the basis for numerical analysis. In the numerical procedure, each of the complex equations (32) is represented as a system of two real equations for the mode amplitude

$$\frac{d}{dt}E_k(t) = \frac{v_g}{2}g_k^{\rm net}E_k(t) + {\rm Re}\left[e^{-i\varphi_k}\sum_m G_m(t)\cdot\widetilde{\rm E}_{k+m}(t)\right] \tag{42}$$

and phase

$$\frac{d}{{\rm dt}}\varphi_k(t) = \omega_k^i - \omega_k^n \tag{43}$$

Here, the real variable

$$\omega_k^i = \Omega_k + {\rm Im}\left[\frac{1}{\widetilde{\rm E}_k}\sum_m G_m(t)\cdot\widetilde{\rm E}_{k+m}(t)\right] \tag{44}$$

has the meaning of an instantaneous mode frequency (in the steady state, the right-hand side of (43) vanishes so that the instantaneous frequency equals the nominal frequency). Using the moderate dispersion approximation, we can express the net modal gain in (42) in a form similar to standard rate equations

$$g_k^{\rm net} = \Gamma(f_g g - f_a a) - a_{c0} - (\delta g_k + \delta a_{\rm ck}) \tag{45}$$

where a_{c0} is the cavity loss for the reference mode, $f_{g,a}$ are the volume (length) fractions of the gain and absorber, and the corrections $\delta g_k = f_g(g_0 - g_k) + f_a(a_k - a_0) \ll g, a$ and $\delta a_{\rm ck} = a_{\rm ck} - a_{c0} \ll a_{c0}$ describe the mode selective properties (dispersion) of the active medium and the cavity, respectively. Likewise, in (44)

$$\Omega_k = k\Delta\Omega_0 + \delta\Omega_k, \quad \delta\Omega_k \ll \Delta\Omega_0. \tag{46}$$

Finally, we remove the ambiguity in the definition of mode phases and frequencies by specifying the way of calculating the instantaneous mode interval $\Delta\Omega(t)$ and the reference mode shift $\Omega_{\rm c}(t)$. The former, in the case of purely passive ML, is estimated as

$$\Delta\Omega = \Delta\Omega^i = \frac{\sum_{k>l} E_k E_l \frac{\omega_k^i - \omega_l^i}{k-l}}{\sum_{k>l} E_k E_l}. \tag{47}$$

In the case of active or hybrid ML, we use $\Delta\Omega = \Delta\Omega_{\rm mod} = {\rm const}$ in the integration of (32), though the instantaneous value $\Delta\Omega^i(t)$ is also calculated using (47) and used to characterize the ML transient. The reference mode shift is calculated as

$$\omega_c = \frac{\sum_k E_k^2\left(\omega_k^i - k\Delta\Omega\right)}{\sum_k E_k^2} \tag{48}$$

in both cases.

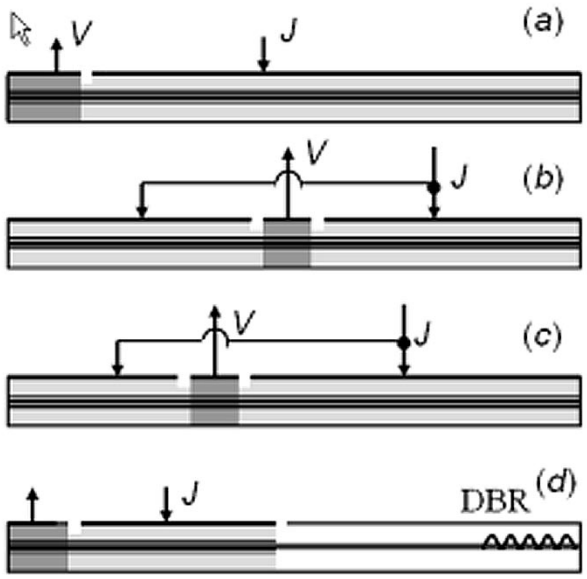

Fig. 1. Laser constructions analyzed in the paper: (a) tandem passively mode-locked laser; (b) colliding-pulse mode-locked laser; (c) single-absorber ACPM laser; and (d) hybridly mode-locked DBR laser. Light filling: gain sections, darker filling-absorber/modulator sections, no filling—passive sections.

III. Application to Different Constructions and Regimes

A. Tandem-Geometry Fabry–Perot Passively Mode-Locked Lasers

In the case of Fabry–Perot lasers [Fig. 1(a)] with a cavity of the length L and length fractions $f_{g,a} = L_{g,a}/L$ occupied by the gain and absorber sections, respectively, the intermodal interval is estimated simply as $\Delta\Omega_0 = v_g/2L$. The instantaneous modal profiles can be calculated analytically (see Appendix), and the exact frequencies and losses of the uncoupled modes in (45) and (46) are given by the usual expressions

$$\delta\Omega_k = \frac{1}{2}k^2\frac{dn_g}{d\omega}\Delta\Omega_0^2 + v_g(f_g\alpha_g g - f_a\alpha_a a) \tag{49}$$

and

$$a_{c0} = \frac{1}{L}\ln\left(\frac{1}{r_R r_L}\right) + a_{\rm int}. \tag{50}$$

The mode selectivity is provided only by the dispersion of the net gain $\bar{g} = f_g g - f_a a$

$$\delta a_k = 0 \qquad \delta g_k = k^2\frac{d^2\bar{g}}{d\omega^2}\Delta\Omega_0^2. \tag{51}$$

The relations above hold regardless of the position of the absorber in the cavity; the SA geometry only enters the rate equations (42) and (43) via the overlap factors (37a) and (37b) in the coupling coefficients G_m. The specific expressions for these factors used in the calculations below are shown in the Appendix. In the simplest case of a tandem laser with a single short ($f_a \ll f_g$) absorber at one of the facets, these expressions are reasonably close to $\xi_m^{(g)} \approx 0.5\, f_g$, $\xi_a^{(m)} \approx f_a$, $m = \pm 1, 2, 3\ldots$

A typical simulated turn-on transient in a tandem mode-locked laser (with gain and SA sections 40 and

TABLE I
MAIN PARAMETERS USED IN THE CALCULATIONS

notation	meaning	value	units
Γ	Confinement factor	0.03	
a_i	Internal (dissipative) loss	2.5	1/cm
n_g	Group refractive index	3.45	
N_0	Transparency carrier density (gain) (absorption)	$1.2\cdot10^{18}$ $2.5\cdot10^{18}$	cm^{-3}
A_g	Gain cross-section, gain absorption	$7\cdot10^{-16}$ $15\cdot10^{-16}$	cm^2
α_g	Linewidth enhancement factor, gain	2	
α_a	Linewidth enhancement factor, SA FP laser DBR	 0.5 1	
ε_g	Gain compression coefficient	$4\cdot10^{-17}$	cm^3
ε_g	Absorption compression coefficient, FP and DBR CPM ACPM	 $7\cdot10^{-17}$ $15\cdot10^{-17}$ $18\cdot10^{-17}$	cm^3
τ_a	Nonradiative recombination time (absorber)	8	ps
B	Bimolecular recombination coefficient	$2.5\cdot10^{-10}$	cm^6/s
τ_{nr}	Nonradiative recombination time (gain)	10	ns
$\Delta\Omega$	Gain spectrum width parameter	$5\cdot10^{13}$	1/s

500 μm, respectively, the other main parameters are summarized in Table I) is shown in Fig. 2. Note that intensities of individual modes see a relatively slow oscillatory relaxation, due to supermode competition, after the faster electron-photon relaxation oscillations of the total intensity has settled down; the same supermode relaxation transient is experienced by phases and, therefore, by the instantaneous intermodal interval. The resulting steady-state spectrum [Fig. 3(a)] shows both a noticeable asymmetry, with a steeper red edge, and a significant red shift—both may be explained by the self-phase modulation, mainly in the gain section of the laser. For comparison, a dashed line shows the spectral envelope for the same laser calculated using a distributed time-domain model [1] (produced by Fourier transforming a single ML pulse). A good agreement between the two models can be achieved, though the gain bandwidth in the time-domain simulation needed to be taken somewhat smaller than that of the mode decomposition approach. The model presented here allows for calculations about an order of magnitude faster than our version of the time-domain model. Recombining the amplitudes and phases allows the temporal pulse profile to be calculated [Fig. 3(b)]. The pulse shape and duration obtained by the two models are in good agreement.

B. Colliding-Pulse and Asymmetric-Colliding-Pulse Passive ML

Passive colliding-pulse ML (CPM) is a well-known method for achieving stable, short pulses by placing a single saturable absorber in the middle of the Fabry–Perot cavity [Fig. 1(b)], resulting in a doubling of the repetition rate compared to the tandem construction. When applying our model to a CPM laser, the relations (49)–(51) still hold, but the expressions for overlap factors now give approximately $\xi^{(a)}_{2m} \approx f_a$, $\xi^{(a)}_{2m-1} \approx 0$. As a result, modes with odd numbers die out

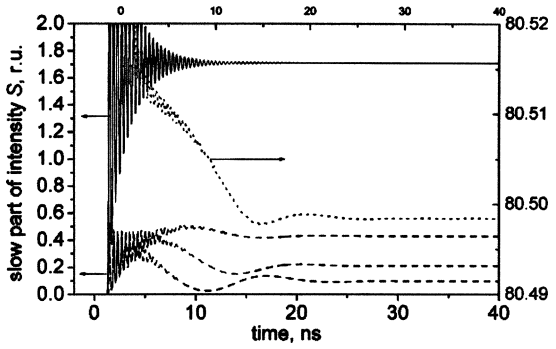

Fig. 2. Simulated turn-on transient in a tandem mode-locked laser with a single saturable absorber as in Fig. 1(a). Top curve (solid): total intensity; middle curve (dotted): instantaneous intermodal interval; bottom curves (dotted): intensities of individual modes (top to bottom): -3, -2, -1.

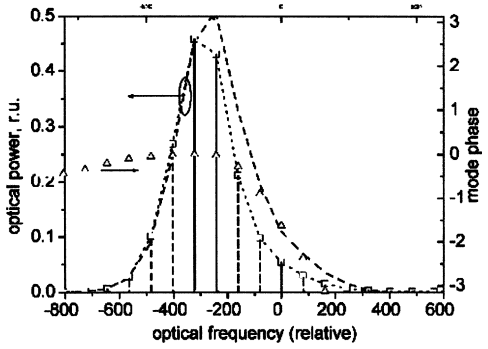

(a)

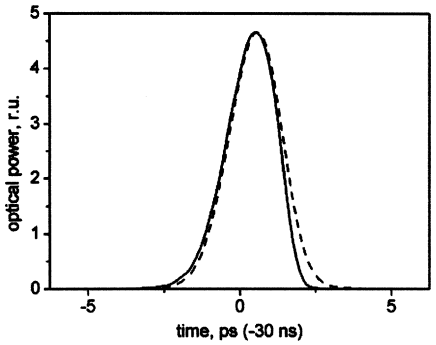

(b)

Fig. 3. (a) Steady state spectrum and (b) temporal pulse profile for a laser presented in the previous figure. Solid: the present model. Dashed: fully time-domain simulation. Scattered points in Fig. 2(a) are mode phases.

during the initial relaxation oscillations immediately following switch-on, leaving only modes with even numbers in the resulting steady-state spectrum [Fig. 4(a)]. In the time domain, this corresponds [Fig. 4(b)] to a pulse train with a repetition rate of $2F$ ($F = \Delta\Omega/2\pi$), with subpicosecond durations and modest chirp, in agreement with the experimental trends. We note, though, that in simulations with different parameters, we observed significant competition between the "even" and "odd" CPM supermodes, and even situations when the repetition frequency doubling was achieved without the doubling of the intermodal interval, purely due to there being a phase shift of $\approx \pi$ between even and odd modes. As has been shown by the time-domain simulations [10], transient gratings not included in the current version of our model can further stabilize the dominant supermode.

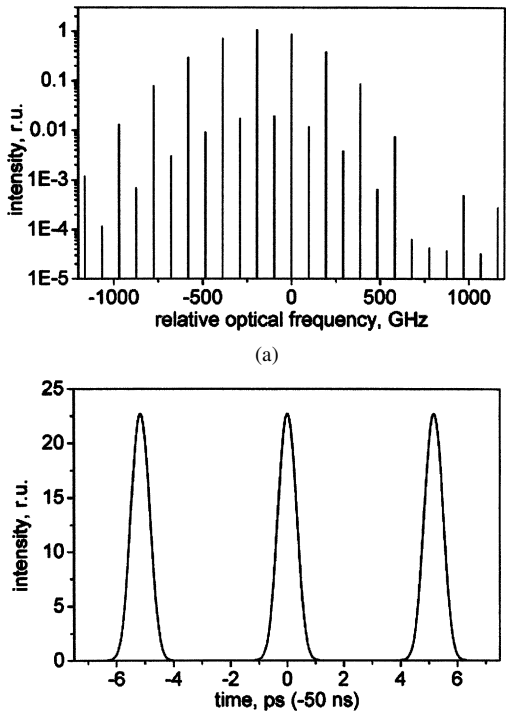

Fig. 4. (a) Steady-state spectrum of a CPM laser 430 μm long, with the saturable absorber 30 μm long. (b) fragment of the corresponding pulse train (1.5 round-trips of the fundamental laser cavity).

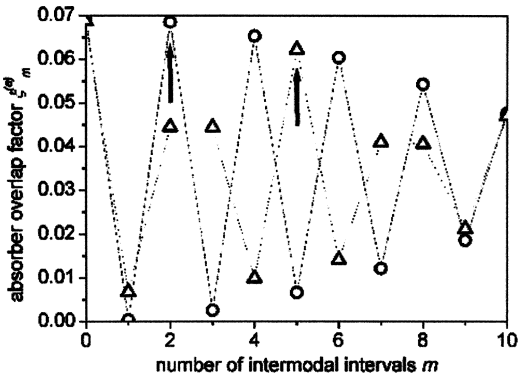

Fig. 5. Mode overlap factors $\xi_m^{(a)}$ for CPM (circles) and ACPM (triangles) lasers. Dotted lines are purely to guide the eye, arrows indicate the position of the lasing harmonic. In both cases, the laser is 430 μm long, with the saturable absorber 30 μm long positioned at the middle (CPM) or at 2/5 of length (ACPM).

An important generalization of the CPM principle involves positioning either one short absorber section [asymmetric CPM (ACPM)] or several absorbers [multiple CPM (MCPM)] within the laser cavity at a distance of L/M $(M = 3, 4 \ldots)$ from a facet and/or from each other, leading under properly adjusted bias conditions to ML with a repetition rate of MF. The physics of MCPM operation was explained [13] using an earlier version of the present model (without fully solving the rate equations). Since then, ML at record repetition rates of 500–800 GHz has been achieved using a modification of ACPM with a single SA at a distance $M_1/M \cdot L$ (e.g., 2/5 or 5/12) from the facet. Here, we model a laser with a geometry

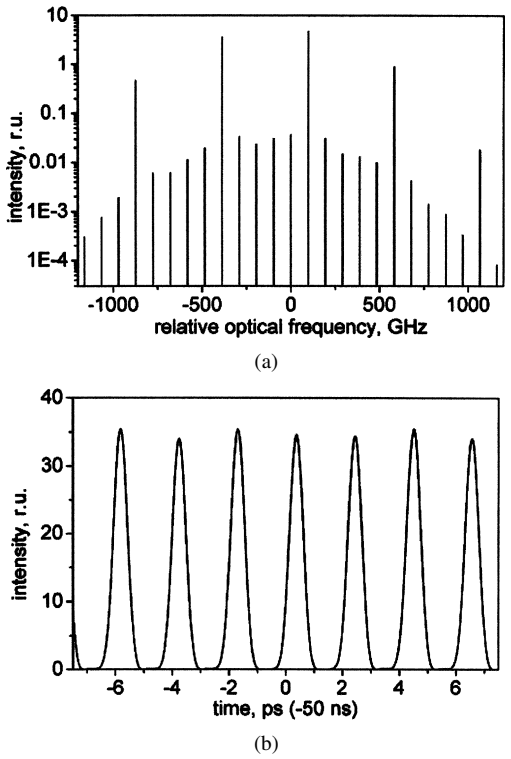

Fig. 6. (a) ML spectrum and (b) fragment of the corresponding pulse train (1.5 round-trips of the fundamental laser cavity) for an ACPM laser, geometry as in Fig. 6.

of this type [F =100 GHz, $M_1 = 2$, $M = 5$, Fig. 1(c)]. As in all Fabry–Perot constructions, the "cold-cavity" mode frequencies and losses are given by (49)–(51), with the harmonic operation ensured by the overlap factors $\xi_m^{(a)}$. The values of these parameters are shown in Fig. 5. For comparison, the values for the CPM laser treated in the previous example are also shown. In the case of ACPM laser, as in the case of MCPM lasers studied in [13] and, unlike the case with simple CPM, the coefficients $\xi_m^{(a)}$ are significant even for $|m| < M$. However, with strong enough mode coupling, numerical simulations of the rate equations still yield a steady-state spectrum with the nonharmonic "satellite" modes suppressed by about 30 dB [Fig. 6(a)], which corresponds in the time domain to a stream of pulses with a repetition rate of MF (in our case, 500 GHz) with little visible subharmonic modulation [Fig. 6(b)].

The alternative means of ML at ultrahigh rates, using frequency-selective compound cavities, may also be analyzed using this model and have been reported elsewhere [25], [35].

C. DBR Lasers

Mode-locked DBR lasers are attracting considerable attention as optical sources for a number of applications (see [1] for an overview). The optical spectrum in ML DBR lasers is naturally limited by the Bragg stopband and includes only a small number of modes, which makes our model particularly well suited for treating these lasers—after appropriate modifications. Consider for example a commonly used construction shown in Fig. 1(d) and consisting of a SA section with a length L_a, a gain section with a length L_g, an optically passive section with a length L_p (including the phase adjustment section if any),

and the DBR section with an optical frequency dependent complex reflectance $r_B(\omega) = |r_B|\exp(i\phi_B)$. The effective cavity length of such a laser is

$$L_{\text{eff}} = L_a + L_g + L_p + L_{\text{refl}} \tag{52}$$

Here, the last term is the effective reflection length in the Bragg mirror [36]

$$L_{\text{refl}} = \frac{v_g}{2}\frac{\partial \phi_B}{\partial \omega}. \tag{53}$$

In the simplest case of a lossless DBR of a large length $L_{\text{Bragg}} \gg 1/K$, $K = K_{\text{rl}} = K_{\text{lr}}$ being the coupling coefficient, $|r_B(\omega_{\text{Bragg}})| = |r_{B0}| \approx \tanh(KL_{\text{Bragg}})$ at the Bragg wavelength ω_{Bragg} (which is taken to approximately coincide with the reference frequency) and $L_{\text{refl}} \approx 1/(2K)$; for more general expressions see, for example, [36]. The effective cold-cavity round-trip frequency is now $\Delta\Omega_0 = v_g/2L_{\text{eff}}$, and the expressions for the overlap coefficients are also modified, with L in (37a), (37b), and (38) and in the formulas in the Appendix being substituted by L_{eff}.

The effective net modal losses and frequencies are now calculated by solving the characteristic equation for the laser cavity [36] self-consistently, so that

$$a_{c0} = \frac{1}{L}\ln\left(\frac{1}{|r_{B0}|r_L}\right) + a_{\text{int}} \tag{54}$$

and both the dispersion of modal frequency and that of loss (the cavity selectivity) are dominated by the effects of the DBR cavity

$$\delta\Omega_k = \frac{\Delta\Omega}{2\pi}\left(\phi_B(\omega_k) - \phi_{B0}\right) \tag{55}$$

$$\delta a_{\text{ck}} = \frac{1}{L}\ln\left|\frac{r_{B0}}{r_B(\omega_k)}\right| \gg \delta g_k. \tag{56}$$

Here, we shall consider a laser similar to those used for communications-related applications, i.e., designed for operation at approximately 40 GHz. We consider a structure as in Fig. 1(d), with the SA, gain, and passive sections 80, 600, and 340-μm long, respectively, followed by a DBR section with the coupling coefficient $(\text{K} = 80\ 1/\text{cm})$ chosen to select about five longitudinal modes. For the purely passive ML in a DBR laser, the model does indeed predict a grating-bandwidth limited spectrum with typically four to five modes, corresponding to a spectral width of several picoseconds (Fig. 7, dashed curve). Of particular interest for practical purposes, however, is the case of hybrid ML with a modulation applied to the absorber contact of the laser, described in the following section.

D. Hybrid ML, Locking Ranges, and Mechanisms

Here, as in [12], we assume that the absorber modulation is proportional to the voltage modulation and, therefore, approximately sinusoidal. Then, in the expressions (36) for mode interaction coefficients $\Delta a_{\pm 1} > 0$ but $\Delta a_{\pm 2,3,\ldots} = 0$. Unless specified otherwise, this section considers a DBR laser with parameters and approximations as discussed in the previous section. For such a laser, as seen in Fig. 7, the pulsewidth decreases with absorption modulation amplitude, as expected. This is accompanied by a slight increase in the grating-bandwidth-limited spectrum width (this is difficult to accurately quantify though, due to only a few modes' being present in the spectrum); the time-bandwidth product remains modest (of the order of 0.5) implying modest chirp at all operating conditions.

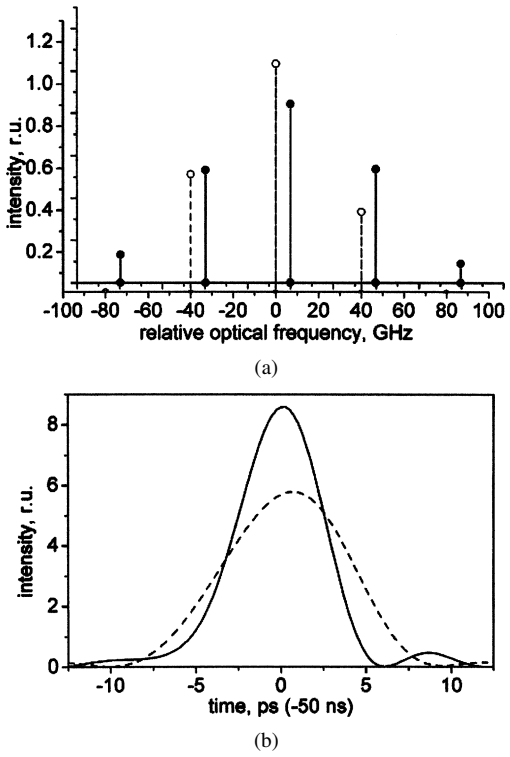

Fig. 7. (a) ML pulse shapes emitted by a passively or hybridly mode-locked DBR laser and (b) the corresponding spectra. Dashed lines/empty symbols: passive ML. Solid lines/filled symbols: pronounced hybrid ML ($a_{mod}/a_c = 0.024$ at $F_{\text{mod}} = 39.82$ GHz).

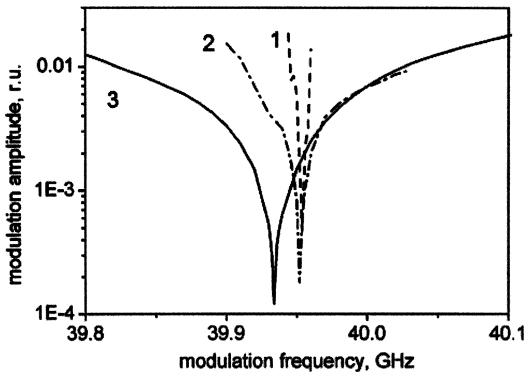

Fig. 8. Locking range of hybrid ML. (1): Fabry–Perot laser, full 35-mode spectrum simulated; (2): same laser with only 5 modes taken into account; (3) DBR laser as in Fig. 7.

The efficiency of our model when applied to slow transients, particularly in a laser with only a few modes such as a hybridly mode-locked DBR laser, allows us to investigate the locking range of hybrid ML more efficiently than it was possible with a fully time-domain model [12]. To do so, we study the time evolution of the instantaneous modal interval $\Delta\Omega_i$ and consider the laser operation locked if the value of $\Delta\Omega_i(t)$ settles at $\Delta\Omega_i = \Delta\Omega_{\text{mod}}$ and unlocked otherwise. The range of parameters (modulation amplitude vs. frequency detuning between modulation and passive ML frequency) in which the locking is observed is plotted in Fig. 8 for different laser constructions. As in the experimental observations, the locking

range is asymmetric, slowing the laser down being easier than speeding up. For realistically achievable modulation amplitudes, the frequency range for locking is of the order of several per cent of the repetition frequency, also in agreement with the experiments. At very high modulation amplitudes ($\sim$0.1 on the scale of Fig. 8), the condition $\Delta\Omega_i = \Delta\Omega_{mod}$ holds, but self-pulsation gradually sets in, which may contribute to the increase of noise under large-signal modulation observed under some experiments.

The modal dynamics approach allows us to identify different factors that affect the locking range. To start with, we compare the locking properties of a hybridly mode-locked DBR laser with those of a Fabry–Perot laser of approximately the same effective (in the case of a Fabry–Perot laser, physical) length and with the same lengths of the amplifier and absorber sections. Such a laser, like the DBR laser, can be locked to an external signal (Fig. 8, dashed curve 1), but in a frequency range much narrower than that of a DBR laser. Unlike the case of a DBR laser, hybrid mode-locked operation of a Fabry–Perot laser is accompanied by a strong shift of the lasing spectrum compared to the passive ML, approximately proportional to the detuning between the hybrid and passive ML repetition rate. This shift was also registered in our time-domain simulations [12]. With the large group velocity dispersion (GVD) values used in [12], the magnitude of the shift was consistent with the spectrum peak moving so that the hybrid ML rate would match the frequency-dependent intermodal interval. The GVD values used here, however, are too small to explain the shift entirely by this mechanism. We conclude that the nonlinear interaction between pulse chirp and the shaping effect of the modulation must also play a significant role. Still, we find that the dispersive properties of the resonator do play a part in determining the locking range. To prove this, we use the unique possibilities of our model to simulate a hypothetical structure which, like a DBR laser, has a restricted spectrum, but with little or no intermodal interval dispersion. It is, essentially, a Fabry–Perot cavity with the number of modes artificially restricted to five in our case. In this case (dash-dotted curve 2), the locking range is broadened considerably when compared to the Fabry–Perot laser, but still narrower than that of the true DBR (solid curve 3). We conclude, therefore, that the broad locking range of the DBR laser compared to the FP cavity is due to a combination of the restricted spectrum (lowering the ML "oscillator quality" and thus easing the locking) and the grating-caused dispersion of the intermodal interval. The latter is most important for repetition rates *lower* than that of the free-running passive ML—in this case, the spectral broadening as in Fig. 7 involves excitation of outer modes of the spectrum which have smaller intermodal intervals due to dispersion. This brings the instantaneous intermodal interval closer to the modulation frequency and thus facilitates locking.

Fig. 9 gives some examples of the dynamics of the instantaneous power S and the instantaneous modal interval $\Delta\Omega_i$ in a DBR laser after the modulation is applied. In the case of modulation amplitude high enough to achieve locking (the solid curve 1 in Fig. 9), the transient consists of relaxation oscillations (much more pronounced in the intensity variation than in that of the intermodal interval), accompanied or followed by a slower transient, several nanoseconds long (the time constant identified in the previous studies as the supermode relaxation time), during

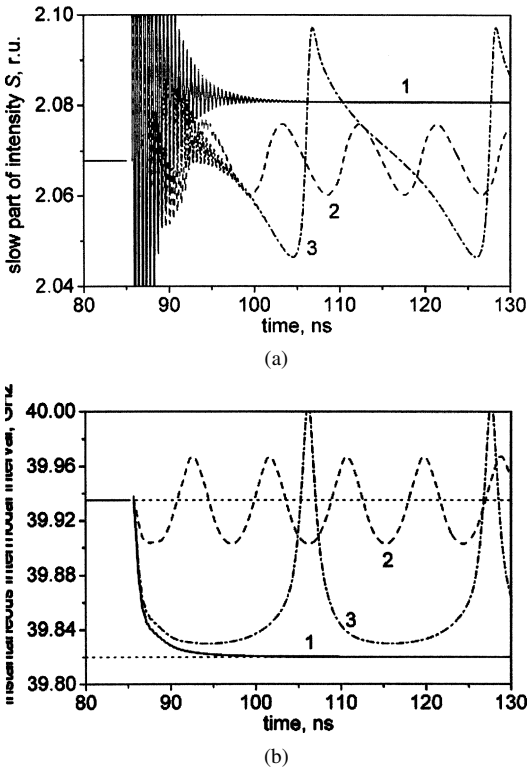

Fig. 9. (a) Transient behavior of the instantaneous power and (b) intermodal interval in a mode-locked DBR laser under external periodical excitation. External modulation at $F_{\rm mod} = 39.82$ GHz switched on at $t = 85$ ns. Successful locking: solid curve (1): $a_{\rm mod}/a_c = 0.011$; unsuccessful locking: dashed curve (2): $a_{mod}/a_c = 0.003$ and dash-dotted curve (3): $a_{mod}/a_c = 0.0095$. Dotted lines show the free-running repetition frequency (39.935 GHz) and the modulation frequency.

which the intensity and period relax to their steady-state values, in agreement with earlier time-domain simulations. In the opposite case of very small modulation amplitude (the dashed curve 2), we observe an almost sinusoidal variation of both intensity and repetition period at the frequency (nearly) equal to the difference of repetition frequencies of free-running (passive) and active ML, with the average repetition period very close to that of passive ML. This is the frequency mixing regime observed in our previous time-domain simulations [12]. In the intermediate case of modulation strong enough to cause significant pulling of the repetition frequency toward the modulation frequency but still too weak to achieve locking, the laser approaches the locked state but never reaches it, with the near-synchronization being periodically lost (the dash-dotted curve 3 in Fig. 9). A very similar behavior was, again, seen in our time-domain simulations [12] and called quasi-locking instability. The closer the operating point is to locking, the longer are the quasi-locked periods of operation. Mathematically, such behavior of a dynamic system is consistent with a saddle-node bifurcation on a periodic orbit [37]; the application of the dynamic modal approach to more detailed analysis of the (in)stability properties of mode-locked lasers is reserved for future work.

IV. Summary and Conclusion

In summary, we have presented a modal decomposition based model applicable to a number of multimode and mode-locked

laser structures. The main approximations essential for this approach have been identified as weak modulation/nonlinearity and moderate dispersion. Whilst these approximations, particularly the former, do limit the applicability of the approach (e.g., it becomes problematic for high-power, long cavity lasers), we believe the model presented here can accurately describe a large number of practically relevant laser constructions and experimental situations. We believe the results obtained on harmonic ML (e.g., ACPM considered here and compound-cavity lasers treated in [25] and [35]) and on passive and hybrid mode-locked DBR lasers show that modal analysis is, at the very least, a very useful supplement for time-domain simulations and in some cases may substitute these completely. We believe our approach offers a unique insight into some of the factors responsible for laser properties, allowing us, for example, to isolate the role of reflection bandwidth and dispersion in determining the locking properties of a hybridly mode-locked DBR laser. Finally, the modal dynamics approach can offer an improvement of 1–2 orders of magnitude in calculation speed over time-domain simulations, particularly for lasers with a restricted spectrum.

Further developments of the model may include the study of noise properties and of optical injection, which is relevant to WDM applications. Another attractive further application of the modal decomposition approach would be a systematic study of instabilities in mode-locked lasers. These present a challenge for both experimental studies and time-domain theories but can be relatively straightforwardly studied using the present model by applying the well-established mathematical apparatus such as stability criteria for steady-state solutions of systems of ordinary differential equations.

APPENDIX
WAVE FUNCTIONS AND OVERLAP COEFFICIENTS

In Fabry–Perot or DBR lasers, which have no active gratings and no internal reflectors, the solution of (14) with (12) and (13) gives wave functions in all the active (gain and SA) sections in the simple form

$$U_k = \left\{ \begin{array}{c} \frac{\rho_L}{N} \exp\left(-i \int\limits_{-\frac{L}{2}}^{z} q_k(z')\mathrm{d}z' \right) \\ \\ \frac{1}{N} \exp\left(i \int\limits_{-\frac{L}{2}}^{z} q_k(z')\mathrm{d}z' \right) \end{array} \right\}.$$

Here, the complex propagation factors $q_{\mathrm{k}}(z)$ within the amplifier sections are

$$q_k = \frac{\widetilde{\Omega}_k}{v_g} + \frac{\Delta\eta\omega}{v_g} + i\frac{g_k}{2}$$

with $\Delta\eta$ describing the carrier dependent refractive index; in the SA sections, g_k is substituted by $(-a_k)$. The normalization factor N is chosen to satisfy (16). Then, we split the length of the laser into segments over which the properties of the active layer are assumed constant as discussed in the main text, with L_l and z_l the length and the left coordinate of the lth section (starting with $z_1 = -L/2$). Using (46) and the moderate dispersion approximation, we can approximate within each lth section: $q_{kl} = q'_{kl} + iq''_{kl} \approx (\pi k/L) + i(\gamma_l/2)$, with $\gamma_l \approx g$, $\gamma_l \approx -\alpha$ in the gain and SA sections respectively. Then, the integrals in (37a) and (37b) can be evaluated to calculate the overlap factors for Fabry–Perot lasers

$$\xi_m^{(g)} = \sum_{l\in g} \xi_{\mathrm{lm}} \qquad \xi_m^{(a)} = \xi_{\mathrm{lm}}\big|_{l\in a}$$

where the overlaps over individual sections are evaluated as

$$\xi_{\mathrm{lm}} = \frac{1}{N^2 L}\left\{ \frac{H_{l0}-1}{\widetilde{\gamma}_{l0}} \left(\prod_{p=1}^{l-1} H_{p0} + \frac{1}{\rho_L^2} \prod_{p=1}^{l} \frac{1}{H_{p0}} \right) + \frac{H_{\mathrm{lm}}-1}{\widetilde{\gamma}_{\mathrm{lm}}} \left(\prod_{p=1}^{l-1} H_{\mathrm{pm}} + \frac{1}{\rho_L^2} \prod_{p=1}^{l} \frac{1}{H_{\mathrm{pm}}} \right) \right\}$$

where we have, for brevity, denoted $\widetilde{\gamma}_{\mathrm{lm}} = \gamma_l + i((2\pi m)/L)$; $H_{\mathrm{lm}} = \exp(\widetilde{\gamma}_{\mathrm{lm}} L_l)$. The normalization factor N is then

$$N = \frac{1}{L}\sum_{all\ l}\left\{ \frac{H_{l0}-1}{\widetilde{\gamma}_{l0}} \left(\prod_{p=1}^{l-1} H_{p0} + \frac{1}{\rho_L^2} \prod_{p=1}^{l} \frac{1}{H_{p0}} \right) \right\}.$$

The expressions above are similar to those used in [13], except that, in the present paper, we have only considered lasers with one saturable absorber section (for the MCPM lasers that have several SAs, the summation over l should apply to the SA region as well, as in [13]). For DBR lasers, the length L is substituted by the effective length L_{eff} (52).

ACKNOWLEDGMENT

One of the authors, E. A. Avrutin, wishes to thank E. L. Portnoi and K. A. Shore for useful discussions at various stages of the work.

REFERENCES

[1] E. A. Avrutin, J. H. Marsh, and E. L. Portnoi, "Monolithic and multi-GHz mode locked semiconductor lasers: experiment, modeling and applications," *Proc. IEE Optoelectron.*, vol. 147, no. 4, pp. 251–278, 2000.

[2] R. G. M. P. Koumans and R. Van Roijen, "Theory for passive mode-locking in semiconductor laser structures including the effects of self-phase modulation, dispersion and pulse collisions," *IEEE J. Quantum Electron.*, vol. 32, pp. 1782–1790, Mar. 1996.

[3] J. A. Leegwater, "Theory of mode-locked semiconductor lasers," *IEEE J. Select. Topics Quantum Electron.*, vol. 32, pp. 1782–1790, Oct. 1996.

[4] S. Arahira and Y. Ogawa, "Repetition-frequency tuning of monolithic passively mode-locked semiconductor lasers with integrated extended cavities," *IEEE J. Quantum Electron.*, vol. 33, pp. 255–265, Feb. 1997.

[5] V. B. Khalfin, J. M. Arnold, and J. H. Marsh, "A theoretical model of synchronization of a mode-locked laser with an external pulse stream," *IEEE J. Select. Topics Quantum Electron.*, vol. 1, pp. 523–527, June 1995.

[6] J. L. A. Dubbeldam, J. A. Leegwater, and D. Lenstra, "Theory of mode-locked semiconductor lasers with finite absorber relaxation times," *Appl. Phys. Lett.*, vol. 70, no. 15, pp. 1938–1940, 1997.

[7] P. A. Morton, R. J. Helkey, and J. E. Bowers, "Dynamic detuning in actively mode-locked semiconductor lasers," *IEEE J. Quantum Electron.*, vol. 25, pp. 2621–2633, Dec. 1989.

[8] M. Schell, A. G. Weber, E. Schöll, and D. Bimberg, "Fundamental limits of sub-ps pulse generation by active mode locking of semiconductor lasers: The spectral gain width and the facet reflectivities," *IEEE J. Quantum Electron.*, vol. 27, pp. 1661–1668, June 1991.

[9] W. Yang and A. Gopinath, "Study of passive mode locking of semiconductor lasers using time-domain modeling," *Appl. Phys. Lett.*, vol. 63, pp. 2717–2719, 1993.

[10] L. M. Zhang and J. E. Carroll, "Dynamics response of colliding-pulse mode-locked quantum-well lasers," *IEEE J. Quantum Electron.*, vol. 31, pp. 240–242, Feb. 1995.

[11] M. Schell, M. Tsuchiya, and T. Kamiya, "Chirp and stability of mode-locked semiconductor lasers," *IEEE J. Quantum Electron.*, vol. 32, pp. 1180–1190, July 1996.
[12] E. A. Avrutin, J. M. Arnold, and J. H. Marsh, "Analysis of dynamics of monolithic passively mode-locked laser diodes under external periodic excitation," *Proc. IEE Pt. J.*, vol. 143, pp. 81–88, 1996.
[13] J. F. Martins-Filho, E. A. Avrutin, C. N. Ironside, and J. S. Roberts, "Monolithic multiple colliding pulse mode locked quantum well lasers: experiment and theory," *IEEE J. Select. Topics Quantum Electron.*, vol. 1, pp. 539–552, June 1995.
[14] H. Haus, "A theory of forced mode-locking," *IEEE J. Quantum Electron.*, vol. QE-11, pp. 323–330, July 1975.
[15] K. Y. Lau, "Efficient narrow-band direct modulation of semiconductor lasers at millimeter wave frequencies of 100 GHz and beyond," *Appl. Phys. Lett.*, vol. 52, pp. 2214–2216, 1988.
[16] ——, "Narrow-band modulation of semiconductor lasers at millimeter wave frequencies (>100 GHz) by mode locking," *IEEE J. Quantum Electron.*, vol. 26, pp. 250–261, Feb. 1990.
[17] J. Paslaski and K. Y. Lau, "Parameter ranges for ultrahigh frequency mode locking of semiconductor lasers," *Appl. Phys. Lett.*, vol. 59, pp. 7–9, 1991.
[18] K. Y. Lau and J. Paslaski, "Condition for short pulse generation in ultrahigh frequency mode locking of semiconductor lasers," *Photon. Technol. Lett.*, vol. 3, pp. 974–976, 1991.
[19] O. Solgaard, M.-H. Kiang, and K. Y. Lau, "Pulse buildup in passively mode-locked monolithic quantum-well semiconductor lasers," *Appl. Phys. Lett.*, vol. 63, pp. 2021–2023, 1993.
[20] I. Kim and K.-Y. Lau, "Frequency and timing stability of mode-locked semiconductor-lasers—passive and active-mode locking up to millimeter-wave frequencies," *IEEE J. Quantum Electron.*, vol. 29, pp. 1081–1090, Apr. 1993.
[21] E. A. Avrutin, J. M. Arnold, and J. H. Marsh, "Analysis of modal dynamics of monolithic mode-locked semiconductor lasers," presented at the OSA Annu. Meeting, Baltimore, MD, Oct. 5–12, 1998.
[22] R. A. Salvatore, S. Sanders, T. Schrans, and A. Yariv, "Supermodes of high-repetition-rate passively mode-locked semiconductor lasers," *IEEE J. Quantum Electron.*, vol. 32, pp. 941–952, Nov.-Dec. 1996.
[23] M. Lecce and I. Montrosset, "Analysis of integrated mode-locked semiconductor lasers: spectral domain approach," *Proc. IEE Optoelectron.*, vol. 148, pp. 266–272, 2001.
[24] E. A. Avrutin, J. H. Marsh, J. M. Arnold, T. F. Krauss, H. Pottinger, and R. M. De La Rue, "Analysis of harmonic (sub-)THz passive mode locking in monolithic compound cavity Fabry–Perot and ring laser diodes," *Proc. IEE Optoelectron.*, vol. 146, no. 1, pp. 55–61, 1999.
[25] D. A. Yanson, M. W. Street, S. D. McDougall, I. G. Thayne, J. H. Marsh, and E. A. Avrutin, "Ultrafast harmonic mode-locking of monolithic compound-cavity laser diodes incorporating photonic-bandgap reflectors," *IEEE J. Quantum Electron.*, vol. 38, pp. 1–11, Jan. 2002.
[26] H. Wenzel, U. Bandelow, H.-J. Wunsche, and J. Rehberg, "Mechanisms of fast self pulsations in two-section DFB lasers," *IEEE J. Quantum Electron*, vol. 32, pp. 69–78, Jan. 1996.
[27] U. Feiste, "Optimization of modulation bandwidth in DBR lasers with detuned Bragg reflectors," *IEEE J. Quantum Electron.*, vol. 34, pp. 2371–2379, Dec. 1998.
[28] U. Bandelow, "Private Communication," unpublished, 1996.
[29] W. A. Hamel and J. P. Woerdman, "Nonorthogonality of the longitudinal eigenmodes of a laser," *Phys. Rev. A*, vol. 40, no. 5, pp. 2785–2787, 1989.
[30] W. E. Lamb, "Theory of an optical maser," *Phys. Rev.*, vol. 134, pp. A1429–A1450, 1963.
[31] K. A. Shore and W. M. Yee, "Theory of self-locking FM operation in semiconductor-lasers," *Proc. IEE Optoelectron.*, vol. 138, no. 2, pp. 91–96, 1991.
[32] W. M. Yee and K. A. Shore, "Multimode analysis of self locked FM operation in laser-diodes," *IEE Proc. Optoelectron.*, vol. 140, no. 1, pp. 21–25, 1993.
[33] A. Mecozzi and J. Mork, "Saturation effects in nondegenerate four-wave mixing between short optical pulses in semiconductor laser amplifiers," *IEEE J. Select. Topics Quantum Electron.*, vol. 3, pp. 1190–1207, May-June 1997.
[34] E. A. Avrutin, "Analysis of spontaneous emission and noise in self-pulsing laser diodes," *Proc. IEE J. Optoelectron.*, vol. 140, no. 1, pp. 16–20, 1993.
[35] M. W. Street, E. A. Avrutin, D. Yanson, S. D. McDougall, I. G. Thayne, J. H. Marsh, and J. S. Roberts, "Sub-THz passive harmonic mode-locking effects in external reflector compound cavity laser diodes," in *Proc. 12th LEOS Annu. Meeting*, vol. 2, San Francisco, CA, Nov. 8–13, 1999, pp. 703–704.
[36] L. A. Coldren and S. W. Corzine, *Diode Lasers and Photonic Integrated Circuits*. New York: Wiley, 1995, ch. 4.
[37] B. Krauskopf, Private communication, 2002.

Eugene A. Avrutin (M'95) was born in St. Petersburg (then Leningrad), Russia, in 1963. He received the M.Sc. degree with distinction from St. Petersburg Technical University (then Leningrad Polytechnical Institute), St. Petersburg, Russia, in 1986 and the Ph.D. degree from A.F. Ioffe Physico-Technical Institute, St. Petersburg, Russia, in 1994.

From 1986 to 1993, he was with the Integrated Optics Laboratory, Ioffe Physico-Technical Institute, working mainly on theory and modeling of spectral, dynamic, and polarization properties of advanced semiconductor lasers. From 1994 to 1999, he was with the Department of Electrical and Electronic Engineering, University of Glasgow, U.K., where his research centred on theoretical and numerical analysis of ultrafast diode lasers and new materials for semiconductor optoelectronics. Since 2000, he has been a member of the academic staff at the Department of Electronics, University of York, York, U.K., where his interests are in theory, modeling, and design of optoelectronic devices, and in advancement of photonic computer-aided design techniques.

John M. Arnold received the B.Eng. in electronic engineering and the Ph.D. degrees from the University of Sheffield, Sheffield, U.K., in 1968 and 1974.

He was a Postdoctoral Research Assistant with the Department of Electronic and Electrical Engineering, Queen Mary College, University of London, London, U.K., from 1974 to 1978. In 1978, he was appointed Lecturer in the Department of Electronic and Electrical Engineering, University of Nottingham, Nottingham, U.K. In 1985, he was appointed Lecturer in the Department of Electronics and Electrical Engineering, University of Glasglow, Glasgow, U.K., where he has been a Professor of Applied Electromagnetics since 1994. He was appointed Head of the Department of Electronics and Electrical Engineering there in April 2003. His research interests concentrate on mathematical methods in applications to optics and electromagnetic wave propagation, particularly in nonlinear guided-wave optics and semiconductor lasers.

He is a Fellow of the Institute of Physics. He is a Member of the URSI Commission B and has served as the U.K. National Representative for URSI Commission B from 1991 to 1996.

John H. Marsh (M'91–SM'91–F'00) received the B.A. degree in engineering and electrical sciences from the University of Cambridge, Cambridge, U.K., in 1977, the M.Eng. degree in solid-state electronics from the University of Liverpool, Liverpool, U.K., in 1978, and the Ph.D. degree for research in the LPE growth and electrical transport properties of InGaAsP alloys from Sheffield University, Sheffield, U.K., in 1982.

He is the Chief Technical Officer with Intense, a company he co-founded in 2000. He is currently seconded to Intense from the University of Glasgow, Glasgow, UK, where he is a Professor of Optoelectronic Systems in the Department of Electronics and Electrical Engineering. He has developed new integration technologies for photonic integrated circuits based on quantum-well devices and quantum-well intermixing, and has built up an extensive program of work on III-V-based photonic integrated circuits for high-speed digital optical communications. He is author or co-author of more than 380 journal and conference papers. His research interests are concerned with linear and nonlinear integrated optoelectronic systems, primarily in semiconductors.

Prof. Marsh is an Elected Member of the LEOS Board of Governors for 3 years commencing January 2001 and is currently LEOS Vice President for Finance and Administration. He is a Member of the Executive Team of the IEE Photonics Network. He is also a Member of the College of the Engineering and Physical Sciences Research Council and of the Council of the Scottish Optoelectronics Association. He is a Fellow of the Institution of Electrical Engineers, the Royal Society of Arts, and the Royal Society of Edinburgh.